Robust Design of a Re-entry Unmanned Space Vehicle by Multi-fidelity Evolution Control

Journal:	*AIAA Journal*
Manuscript ID:	2011-08-J051573.R3
Manuscript Type:	Full Paper
Date Submitted by the Author:	n/a
Complete List of Authors:	Minisci, Edmondo; University of Strathclyde, Department of Mechanical and Aerospace Engineering Vasile, Massimiliano; University of Strathclyde, Department of Mechanical and Aerospace Engineering
Subject Index Category:	40710 Multidisciplinary Design Optimization < 40000 INTERDISCIPLINARY TOPICS, 32600 Optimization Techniques < 30000 GUIDANCE, CONTROL, AND DYNAMICS TECHNOLOGY
Select ONE Subject Index for the Table of Contents. This is where your paper will show up in the Table of Contents:	40000 INTERDISCIPLINARY TOPICS

Robust Design of a Re-entry Unmanned Space Vehicle by Multi-fidelity Evolution Control

Edmondo Minisci[1] and Massimiliano Vasile[2]
University of Strathclyde, Glasgow, G1 1XJ, UK

This paper addresses the preliminary robust design of a small-medium scale re-entry unmanned space vehicle. A hybrid optimization technique is proposed that couples an evolutionary multi-objective algorithm with a direct transcription method for optimal control problems. Uncertainties on the aerodynamic forces and vehicle mass are integrated in the design process and the hybrid algorithm searches for geometries that a) minimize the mean value of the maximum heat flux, b) maximize the mean value of the maximum achievable distance, and c) minimize the variance of the maximum heat flux. The evolutionary part handles the system design parameters of the vehicle and the uncertain functions, while the direct transcription method generates optimal control profiles for the re-entry trajectory of each individual of the population. During the optimization process, artificial neural networks are used to approximate the aerodynamic forces required by the direct transcription method. The artificial neural networks are trained and updated by means of a multi-fidelity, evolution control approach.

Nomenclature

C_D	= drag coefficient
C_E	= sampling hypersurface
C_L	= lift coefficient

[1] Lecturer, Department of Mechanical & Aerospace Engineering, 75 Montrose Street
[2] Reader, Department of Mechanical & Aerospace Engineering, 75 Montrose Street, AIAA Member

$\mathbf{d}$	=	design vector
d_{body}	=	thickness of the structure [m]
d_{ll}	=	Euclidean distance between point in DB_{train} evaluated at current fidelity level of the models and the points evaluated with lower level models
$d_{min,ll}$	=	minimum Euclidean distance to accept points evaluated with lower level models into the database
$d_{min,sl}$	=	minimum Euclidean distance between the sampled trajectory point and the points of the database evaluated with the same fidelity code, to accept the new point into the database
d_{sl}	=	Euclidean distance between point in DB_{train} and the trajectory points extracted by current solutions
d_{TPS}	=	thickness of the TPS skin covering the vehicle [m]
D	=	drag [N]
$\mathbf{DB}_{train}$	=	matrix of points in the database used to train the approximated model
D_v	=	viscous drag [N]
D_w	=	wave drag [N]
E_q, E_D	=	mean values of the maximum heat flux and the orthodromic distance, respectively
Err	=	error function
g	=	gravity acceleration $[m/s^2]$
h	=	altitude [m]
K_e	=	constant term in the heat flux equation $(1.742\ 10^{-4})$
l	=	nominal length of the wave-rider [m]
L	=	lift [N]
L_C	=	fidelity level of the model
L_{det}	=	deterministic value of the lift [N]
L_{TPS}	=	thickness of the TPS at the nose
L_{unc}	=	value of the lift affected by uncertainties [N]
m	=	total mass of the vehicle [kg]
m_{nose}	=	mass of the TPS at the nose [kg]
m_{skin}	=	mass of the TPS covering the vehicle [kg]
m_{st}, m_{TPS}, m_{pl}	=	structural mass, the mass of the TPS and the mass of the payload (avionics and power system), respectively [kg]
Ma	=	Mach number

n = power law exponent for the shape of the waverider

n_k = number of kernels

n_{gcyc} = defines the generation loop in the generation based evolution control approach

n_{gl} = number of generations of the global optimizer, for which the fidelity of the model is increased the upper level

n_{gv} = number of generations for which the real model has to be used for the generation based evolution control approach

n_o = number of trajectory points to extract from each trajectory

n_p = number of collocation points

n_t = maximum number of trajectory point to extract for each generation

n_v = number of individuals to evaluate by true model in the individual based evolution control approach

N = number of trajectory elements

$\dot{q}_{conv}$ = convective heat flux $[W/m^2]$

r_f = upper bound of the constraints on the final radius [m]

r_{min} = lower bound of the constraints on the final radius [m]

r = norm of the position vector with respect to the center of the planet [m]

Re = Reynolds number

R_E = mean radius of the Earth (const. 6.371 10^6 m)

R_n = radius of curvature at the edges of the vehicle [m]

$\mathbf{S}$ = matrix with data of the trajectory

S_n = surface of the TPS nose cone $[m^2]$

S_{TPS} = TPS surface area except that of the nose $[m^2]$

t = time [s]

T = thrust [N]

v = magnitude of the velocity [m/s]

V_n = volume of the nose $[m^3]$

V_∞ = free stream velocity module [m/s]

w = nominal width of the waverider [m]

x = longitudinal coordinate

Greek symbols

α	=	angle of attack [deg]
β	=	oblique shockwave inclination angle of the waverider
γ_v	=	bank angle [deg]
θ	=	center line wedge angle of the waverider
θ_p	=	flight path angle [deg]
λ	=	longitude [deg]
ρ_{body}	=	density of the vehicle structure [kg/m^3]
ρ_{TPS}	=	density of the TPS material
σ_q^2, σ_D^2	=	variance of the maximum heat flux and orthodromic distance, respectively
τ_E	=	MOPED coefficient for the generation of new individuals
ϕ	=	latitude [deg]
ξ	=	heading angle (azimuth of the velocity) [deg]

I. Introduction

The increase in computer performance allows numerical simulation to replace a big portion of experimental tests, and numerical optimization to handle complex multidisciplinary design problems. However, generally only reduced or low-fidelity models are used during the optimization process on sequential machines. Higher fidelity models are used for more detailed investigations of some promising configurations. In order to reduce the duration and cost of the design process and get better solutions from its early stage, it would be desirable to introduce high fidelity models already in the preliminary design phase. Specific techniques are therefore required to efficiently handle computationally expensive, high fidelity models.

Furthermore, in a wide range of problems the system to be designed needs to be optimally controlled during its operational life. In these cases the optimal control component of the design has an impact on the system design component and vice versa. For example, in the case of a re-entry vehicle, the system, i.e. the re-entry vehicle, follows a descent trajectory that needs to be optimally controlled. The outcome of the optimal control problem has an impact on the maximum heat flux that the vehicle has to withstand and ultimately on its design (shape, material, structure, thermal control system). Conversely the system design component has an impact on the solution of the optimal control component because the dynamics changes.

Lastly, given the preliminary nature of the computation, the inclusion of uncertainties would be desirable in order to generate robust solutions and to highlight the sensitiveness of the design to specific parameters. Hence, the idea is to have an approach capable of 1) integrating system design and optimal control, 2) handle models with different levels of fidelity, and 3) efficiently incorporate design uncertainties in the optimization process. Although many authors have addressed each one of these aspects individually or partially combined, currently there are no examples of integration of all of them together.

One decade ago, Tsuchiya and Mori[1, 2] used the integrated design approach, shape plus control law, for the optimization of launch vehicles. Roshanian and Keshavarz[3] adopted an analogous integrated approach for the multi-disciplinary design of a sounding rocket, with response surface method used to approximate the propulsion model. Since the end of 90's, researchers working on the efficiency of optimization processes have been applying meta-modeling techniques to approximate the response of expensive models, with or without the use of multiple different models, with different fidelity levels and costs, during the optimization process[4–9].

This paper presents a novel approach to the preliminary robust design of complex engineering systems, integrating system design and optimal control into a single optimization process. A population of individuals evolves multiple system design solutions in parallel using an Estimation of Distribution Algorithms (EDAs)[10] called MOPED (Multi-Objective Parzen based Estimation of Distribution) algorithm[11, 12]. At every step of the evolution, an optimal control profile is associated to each individual of the population (each system design solution). The optimal control profile is generated by solving an optimal control problem with a direct transcription method, which transcribes continuous optimal control problems into equivalent non-linear programming problems (NLP) by discretizing both states and controls (for more details on transcription methods for optimal control the interested reader can refer to[13]). Uncertainties in the system design parameters are propagated through the model to compute mean and variance of the relevant performance indexes. Mean and variance are then used as objectives for MOPED. Finally, a meta-modeling technique is used to introduce high fidelity information in the optimization loop while maintaining the computational cost at an acceptable level. The balanced mixture of high fidelity, low fidelity and meta-modeling information is handled through an evolution control process[14].

The case study considered in this paper is the robust design of a medium scale Unmanned Space Vehicle (USV). USVs are seen as a test-bed for enabling technologies and as a carrier to deliver and return experiments to and from low-Earth orbit. They are a potentially interesting solution also for the exploration of other planets or as long-range reconnaissance vehicles for Earth observation [15–17].

In [18] the authors describe a similar approach applied to the design of a small scale USV, taking into account the availability of last generation thermal protection systems (TPS) based on ultra-high temperature ceramic materials (UHTC)[19, 20]. Here the integrated design technique is applied to the design of a larger scale USV, and a different treatment of the optimal control component is introduced: a dual trajectory optimization loop generates control law solutions that minimize the maximum heat flux or maximizes the orthodromic distance, during the re-entry phase. Minimization of maximum heat flux is directly linked to the complexity and costs of the vehicle, because if the vehicle is able to follow a minimal heat flux descent corridor, then cheaper and lighter protecting materials, and under-skin structures, could be used. On the other hand, long range gliding is desirable, because it gives the possibility to robustly select the re-entry point. As in [18], here the shape of the vehicle is derived from an ideal wave-rider configuration([21–23]), and its geometry is modified in order to introduce more realistic rounded edges.

An Artificial Neural Network (ANN) approximated model is used as intermediate layer between the dynamics and aerodynamics of the vehicle such that when the values of drag and lift coefficients are required to compute the forces acting on the vehicle the ANN is interrogated instead of running a full CFD simulation. During the optimization process, the aerodynamic database used to generate the meta-model is updated by a multi-fidelity, evolution control approach: a simplified analytical model and a computational fluid dynamic (CFD) one are scheduled during the optimization process in order to efficiently update the database with solutions sampled where optimal solutions are more likely expected[24–28]. In particular, the low-fidelity model (the analytical one in this case) is used to generate samples globally over the range of the design parameters, while the high fidelity one will be used to locally refine the meta-model in later stages of the optimization.

The paper starts with a description of the proposed robust multidisciplinary design approach, together with the meta-modeling integration, the integration of system design and process control and the treatment of model uncertainties, which are the most innovative aspects of the whole approach. In the following section the integrated design approach is applied to a low dimensional rocket ascent problem, then the USV test case is described, with details on the aerodynamic, thermal, mass, and dynamic models of the vehicle, and some preliminary results are presented. A conclusion section summarizes the key findings of this work and suggests some directions for future developments.

II. Robust Multidisciplinary Design Approach

This paper addresses the integrated design of system and process control under uncertainty. In particular, the design process aims at the simultaneous optimization of the shape and trajectory control profiles of an aerospace vehicle. The multidisciplinary design approach proposed in this paper, integrates an evolutionary multi-objective algorithm with a direct transcription method for optimal control problems. An outer multi-objective evolutionary optimization procedure manages the parameters defining the shape of the vehicle and considers as objectives and constraints the mean and variance of the values of the performance indexes coming from an inner optimization processes handling the optimal control problem.

Once a shape is defined by the outer loop, the optimal control problem is solved multiple times, each time optimizing a different performance index. The individual optimization of each performance index responds to the need of optimally designing the vehicle for all extreme operational conditions that could face during its operational lifetime, rather than for an intermediate one.

In fact, during the operational life, the shape is a fixed characteristic of the vehicle, and cannot change during the flight (no morphing technology is considered here), while the control law can be varied during the operational phase to optimize the operational performance. As a consequence, if a given shape has to maximize different and possibly conflicting performance indexes, then it is necessary to compute the best control law for each performance index, because a single optimization, combining the performance indexes (e.g., a weighted sum of single objectives), would yield a shape that is suboptimal in extreme conditions. Mean and variance of the performance indexes are then computed following the procedure described in Sec. II B.

The optimization of the optimal control profile makes use of a data-fitted surrogate model to approximate the dynamic characteristics of the vehicle, such as the aerodynamic forces acting on the vehicle, as functions of the shape of the vehicle and its operational conditions. The training and updating of the approximated model(s) is optimally managed though a multi-fidelity evolution control approach. The following sections describe the different aspects of the approach.

A. Multi-objective Algorithm

The outer Multi-Objective Optimization (MOO) problem is solved with the Multi-Objective Parzen based Estimation of Distribution (MOPED) algorithm[11, 12]. MOPED belongs to the class of Estimation of Distribution Algorithms (EDA)[10]. EDA automatically learn the structure of the search landscape, by explicitly constructing and evolving a probabilistic model of the search space. New candidate solutions are then generate by sampling the probabilistic model.

MOPED is a multi-objective optimization EDA for continuous problems that uses the Parzen method[36] to build a probabilistic representation of Pareto solutions, with multivariate dependencies among variables[11, 12]. MOPED implements the general ranking and selection strategies of the Non-dominated Sorting Genetic Algorithm II (NSGA-II)[35], while solutions are generated by sampling from the Parzen model instead of using the genetic operators in NSGA-II. The Parzen method is a non-parametric approach to kernel density estimation and provides an estimator that converges everywhere to the true Probability Density Function (PDF) in the mean square sense. Should the true PDF be uniformly continuous, the Parzen estimator can also be made uniformly consistent. In short, the method allocates N_{ind} identical kernels (where N_{ind} is the number of individuals of the population of candidate solutions), each one centred on a different element of the sample. By means of the Parzen method, a probabilistic model of the promising search space portion is thus built on the basis of the information given by N_{ind} individuals of the current population, and $\tau_E N_{ind}$ new individuals ($\tau_E \geq 1$) can then be sampled . The variance associated with each kernel depends on (i) the distribution of the individuals in the search space and (ii) the fitness value associated with the pertinent individual, so as to favor sampling in the neighborhood of the most promising solutions.

B. Robust Design Optimization Under Uncertainty

The objectives and constraints of the outer loop are the statistical moments of the performance indexes obtained by solving the inner optimal control problems. In the inner loop, the optimal control problems are solved considering deterministic models. Thus the solution of the optimal control problems provides the deterministic nominal values of the performance indexes.

Once a deterministic solution is available, uncertainties on key dynamic characteristics, such as the aerodynamic forces or the mass, are introduced by perturbing the nominal value of a generic uncertain quantity X_{det}. When uncertainties are related to operational conditions, uncertain values X_{unc} can be obtained as:

$$X_{unc} = X_{det} + Err\ C_E\ X_{det} \tag{1}$$

where Err is an error function, which depends on the operational conditions, and, C_E is a sampling hyper-surface mapping the set of operational conditions into the interval $[-1, 1]$. In the general case, the shape C_E depends on a set of shaping parameters. Later on in this paper C_E will be defined as an interpolating surface whose shape depends on the value of each interpolating node. For each nominal solution of the inner loop, N_s different C_E surfaces are generated by randomly choosing, with uniform distribution in the interval $[-1, 1]$, N_s sets of values for the shaping parameters and then N_s new trajectories are propagated using the perturbed values X_{unc} obtained from Eq. (1). For each point along one of the N_s trajectories, the product $Err\ C_E$ returns a deterministic value in the interval $[-Err, +Err]$. For each of the N_s perturbed trajectories a new value of the performance index is computed and used to calculate the mean E_J and the variance σ_J^2. The two statistical moments for each performance index are then returned to the outer loop.

C. Multi-fidelity Evolution Control

The inner loop needs to evaluate the dynamic models several times both during the solution of the optimal control problem and during the computation of the statistical moments.

In order to make the process computationally affordable, the inner loop interrogates a data-fitted surrogate model instead of the true system model. The data-fitted approximated model is trained and updated during the design process by means of a multi-fidelity evolution control technique.

The basic idea underneath evolution control (EC) is to manage, throughout the optimization process, the evaluation of both the true and the surrogated model in a way that reduces the total computational time but preserving the correctness of the final solution. Due to the necessity to limit the number of training samples, it is very difficult to construct an initial approximated model that is globally correct. Most likely, the approximation will bring the optimization algorithm to false optima, i.e. solutions that are optimal for the approximated model but are suboptimal for the true model. Model management or evolution control techniques address this problem and avoid converging to false optima.

Jin et al.[14] in their paper propose two different approaches for the evolution control of the model: a) individual-based control and b) generation-based control. In the first approach, n_v individuals in the current population are chosen and evaluated with the true model at each generation. In the latter, the whole population is evaluated with the real model, every n_{gcyc} generations, for n_{gv} generations, where $n_{gv} < n_{gcyc}$. The individuals evaluated with the true model are then introduced into a data-set that is used to locally improve the surrogated model.

The method adopted for this work is a mix of both evolution control strategies. Fig. 1 summarizes the whole optimization process. The MOO algorithm MOPED (on the left of Fig. 1, blocks 0a to 4) is integrated with an external procedure that monitors the status of the approximated models (box 6 in Fig. 1). At the end of each iteration (generation), the external procedure checks if an updated version of the approximated model is ready and available. If the approximated model is updated, then all the individuals in the current population are re-evaluated and re-classified with the updated model, before the Parzen distribution is updated and sampled. If the approximated model is not updated, because, for example, a CFD computation is still running, and the difference between the generation of the previous update and the current generation is n_{gcyc}, then MOPED pauses and waits for the new update.

The external procedure also manages, in an asynchronous way, the training and updating of the approximated models. Block 5 in Fig. 1 is detailed in Algorithm 1.

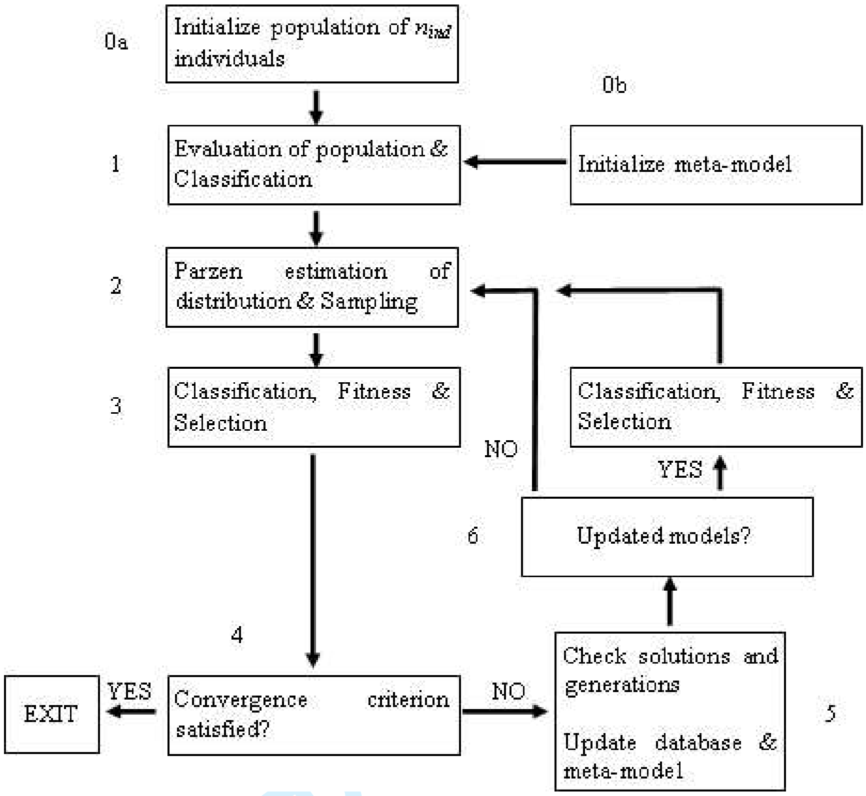

Fig. 1 MOPED with evolution control modification and independent approximated model handler.

The procedure is supplied with a list of system models ordered by increasing level of fidelity and a scheduling report detailing how and when the different models should be used. Every n_{gl} generations of the global solver, the fidelity level of the model, L_C, is increased, till the maximum level, L_{Cmax}, is reached. Then it extracts for each optimal trajectory the matrix $\mathbf{S}_{opt} = [Shape\,parameters,\ Operational\,parameters]$, containing the geometrical parameters and the operative points along the trajectory. Each row in $\mathbf{S}_{opt}$ is then compared to the values in $\mathbf{DB}_{train}$, which is the matrix of points in the database used to train the data-fitted surrogate. The approximated models are initially trained by using the lower fidelity models (fidelity level $L_C = 0$), then during the evolutionary process new promising points are inserted in the database $\mathbf{DB}_{train}$ and used to improve the training. Following a predefined schedule, the level of fidelity is progressively increased from one stage of the evolution to another; therefore the training database will contain a mix of values coming from models at different levels of fidelity. The solutions evaluated with the highest fidelity level are inserted in the database if their distance from all the points of the database evaluated with the same fidelity level, d_{sl}, is greater than a predefined value. Once the higher fidelity solutions are in the database, all lower fidelity solutions falling at a distance $d_{ll} < d_{min,ll}$ from the higher fidelity solutions are discarded. The surrogate structure is then updated with the new data. The data obtained by the higher fidelity models progressively become the main source of updates for the surrogate model till, near the end of the optimization process, the data obtained by the lower fidelity models have no influence in the optimal regions of the search space.

Note that on small scale problems with smooth and differentiable functions a grid search, coupled with a gradient method, could potentially replace the evolutionary optimization process. The grid search, however, would scale exponentially with the number of dimensions and the gradient method would experience difficulties with noisy and discontinuous functions. The proposed robust MDO approach, on the other hand, is composed of strategies and algorithms that scale polynomially with the number of dimensions. In particular, the coupled EC and evolutionary multi-objective optimization algorithm provides an optimal sampling of the true models, and an update of the surrogates, only in the region of interest, thus avoiding the exponential increase of the number of samples required for a global update. Furthermore, the use of a bi-level approach is deemed to be more efficient than the use of a single level approach. In a single level approach the evolutionary process should handle a large number of parameters and constraints and the gradient should search a plethora of inhomogeneous parameters. In the proposed bi-level approach, instead, each technique is applied to the solution of the problem they can handle best.

D. Surrogate Model

General principles of evolution control do not depend on any specific approximation technique but, of course, the approximation approach strongly affects the outcome of any EC strategy. For the particular application presented in this paper, the approximated model should be able to filter the noise coming from the CFD models and correctly generalize the dynamic response for a broad range of shapes and operational conditions. Response surfaces and artificial neural networks were considered[5, 6], but ANNs have been preferred, because they can be used with minimal knowledge

Algorithm 1 Evolution control algorithm

if mod(i_g,n_{gl})=0 & $L_C < L_{Cmax}$ **then**
    $L_C = L_C + 1$
end if
Extract n_o operative points from each individual of the current population ; Put extracted operative points and shapes into $\mathbf{S}_{opt}$
Initialize $\mathbf{DB}_{comp}$=∅ ; Find maximum fidelity level of data in the database $\mathbf{DB}_{train}$, L_{CDBmax}
if $L_C = L_{CDBmax}$ **then**
    Put elements of $\mathbf{DB}_{train}$ with level $= L_C$ into database $\mathbf{DB}_{L_C}$ and elements of $\mathbf{DB}_{train}$ with level $< L_C$ into database $\mathbf{DB}_{L_L}$
end if
if $L_C > L_{CDBmax}$ **then**
    Initialize $\mathbf{DB}_{L_C} = \emptyset$; Put all elements of $\mathbf{DB}_{train}$ into $\mathbf{DB}_{L_L}$
end if
Initialize $i_c = 0$; $i_{pop} = 0$; $\mathbf{DB}_{L_{Cp}} = \mathbf{DB}_{L_C}$
while $i_c < n_t$ & $i_{pop} < size(\mathbf{S}_{opt}, 1)$ **do**
    ipop=ipop+1 ; compute $d_{sl,i}$ [min distance of $\mathbf{S}_{opt}(i_{pop}, :)$ from $\mathbf{DB}_{L_{Cp}}$]
    if $d_{sl,i} > d_{min,sl}$ **then**
        Put $\mathbf{S}_{opt}(i_{pop}, :)$ into $\mathbf{DB}_{L_{Cp}}$; Put $\mathbf{S}_{opt}(ipop, :)$ into $\mathbf{DB}_{L_{comp}}$; $i_c = i_c + 1$
    end if
end while
if $L_C > 0$ **then**
    for i=1:size($\mathbf{DB}_{L_L}$,1) **do**
        compute $d_{ll,i}$ [min distance of $\mathbf{DB}_{L_L}(i, :)$ from $\mathbf{DB}_{L_{Cp}}$]
        if $d_{ll,i} > d_{min,ll}$ **then**
            Put $\mathbf{DB}_{L_L}(i, :)$ into $\mathbf{DB}_{L_C}$
        end if
    end for
end if
Compute function values for operative points and shapes in $\mathbf{DB}_{L_{comp}}$ and insert obtained values in $\mathbf{DB}_{train}$

about the structure of the function, which should be approximated.

When dealing with ANNs, usually radial basis ANNs are preferred due to the modest computational effort required to train them [5, 6], but here the generic Multi Layer Perceptron (MLP) ANN with one hidden layer was used, due to the expected better generalization in regions *far* for the training data.

The training process is based on a Bayesian regularization back-propagation[38], which limits any overfitting problem, and the idea is that the computational costs of initial training and online update are negligible if compared to the calls to the high-fidelity model.

III. Rocket Ascent Case Study

The robust multi-disciplinary design approach, presented in the previous sections, was initially tested on a simple low-dimensional problem with easily verifiable solutions: the design of a vertically ascending single-stage rocket vehicle. The objective of this problem is to find the shape parameters that maximize the expected value of the final altitude and minimize the effect of uncertainties on the aerodynamic forces, given a fixed amount of propellant. The vehicle is considered to be a point mass, whose motion is governed by the following set of dynamic equations ([39], Sec. 8.3):

$$\begin{aligned} \dot{h} &= v \\ \dot{v} &= \frac{T-D}{m} - g \\ \dot{m} &= -\frac{T}{g_0 I_{sp}} \end{aligned} \tag{2}$$

where h is the altitude, v is the velocity, m is the mass of the vehicle, T is the thrust, D the atmospheric drag, g_0 and g the gravity accelerations at sea level and for $h > 0$, respectively, and I_{sp} is the specific impulse. The drag D is given by the classic expression $D = 1/2 \rho C_D S v^2$, where ρ is the atmospheric density, C_D is a shape drag coefficient, and S is a characteristic surface (usually the cross section). The simplifying hypothesis adopted here is that the product $C_D S$ is a known, non-linear function of two shape parameters, $\mathbf{d} = [d_1, d_2]$. The product $C_D S$ is assumed to be uncertain, therefore using Eq. (1), the value of $C_D S$ are perturbed as follows:

$$(C_D S)_{unc} = (C_D S)_{det} + Err\ C_E\ (C_D S)_{det} \tag{3}$$

where Err is a function of speed and altitude and modeled here as a linear 2D surface, with values varying from 0.1, when speed and altitude are both $= 0$, to 0.8, when the speed is $= 2000\ m/s$ and the altitude is $2\,10^5\;m$:

$$Err = 0.000175\,v + 1.75\,10^{-6}\,h + 0.1 \tag{4}$$

while C_E is a multidimensional polynomial spline, interpolating a regular grid of nodes. If $Sp_h(h, \mathbf{s_h})$ and $Sp_v(v, \mathbf{s_v})$ are the splines for altitude and velocity, respectively, then C_E is defined as:

$$C_E = Sp_h(h\mathbf{s_h})\,Sp_v(v, \mathbf{s_v}) \tag{5}$$

where $\mathbf{s_h}$ and $\mathbf{s_v}$ are the values of the splines at the interpolating nodes. $N_{R,h}$ and $N_{R,v}$ equispaced interpolating nodes are taken respectively along the h and v axis. Then N_s values of $\mathbf{s_h}$ and $\mathbf{s_v}$ are randomly sampled in the interval $[-1,\ +1]$ leading to N_s different shapes of C_E. For each shape a varied trajectory is propagated.

Thus, given a nominal trajectory with an optimal control profile T^*, N_s perturbed trajectories are propagated, and the mean E_h and variance σ_h^2 of $\max_t h$ are computed. The mean and variance are then returned as performance indexes to the external loop, which optimizes the shape. The external optimization problem is formulated as follows:

$$\min_{\mathbf{d}\in D}[-E_h,\ \sigma_h^2] \tag{6}$$

The design space for this problem is defined by following bounds on the design parameters: $d_1 \in [0, 2\,\pi]$, and $d_2 \in [0, 20]$.

For the trajectory optimization problem, the control variable is the thrust T, and the control law is computed as the result of the optimal control problem:

$$\max_T h \tag{7}$$

subject to dynamic Eqs. (2) and terminal conditions:

$$\begin{aligned} h(t=0) &= h_0 \\ v(t=0) &= v_0 \\ m(t=0) &= m_0 \end{aligned} \tag{8}$$

$$m(t=t_f) = m_{min} \tag{9}$$

The solution of this optimal control problem is easily verifiable and can be found in ([39], Sec. 8.3). Here, the problem is transcribed with a Gauss pseudo-spectral method[37] to be consistent with the proposed MDO approach. The trajectory is decomposed in N elements, each of which has n_p collocation points. After transcription, the optimal control problem defined by Eq. (7), Eqs. (2) and Eqs. (8, 9) becomes the following nonlinear programming problem:

$$\max_{T_s} h \tag{10}$$

subject to the nonlinear algebraic constraints:

$$C(h_s, v_s, m_s, t_s) = 0 \tag{11}$$

with terminal constraints in Eqs. (8, 9), where $h_s,\ v_s,\ m_s,\ T_s,\ t_s$ are the discrete values of states, control, and time values at the nodes of the transcription scheme.

Trajectories are discretized with 7 elements, and 7 nodes for each element. The bounds on the variables of the trajectory optimization are: total time $T_{tot} \in [0, 1000]$ $[s]$, thrust $T \in [0, 9\,10^4]$ $[N]$, altitude $h \in [0, 2.0\ 10^5][m]$, velocity $v \in [0,\ 2000]$ $[m/s]$, mass $m \in [150, 700]$ $[kg]$. The initial conditions (8) are $x_0 = [h_0,\, v_0,\, m_0]^T = [0,\, 0,\, 700]^T$, while the constraints on the final conditions (9) are $m_f = 150kg$. The initial guess for the control law of every individual is a constant thrust profile with $T = 1kN$. The specific impulse is $I_{sp} = 100s$, while the deterministic values of $C_D S$ are given by the function:

$$C_D S = \left(\frac{(d_2 - 3\, d_1)\, sin(d_2) + (d_1 - 2)^2 + 11}{60} + 0.5 \right) 0.15 \tag{12}$$

Fig. 2(a) shows a three dimensional view of the $C_D S$ as a function of the design parameters, while Fig. 2(b) shows the level curves with the maximum and minimum values for $C_D S$.

A. Rocket Ascent Results

MOPED process was run for 50 generations with a population of 30 individuals. For this simple test case, only one fidelity level has been considered and the characteristic parameters of the evolution control process were set as follows: $n_t = 10$, $n_o = 1$ (the approximated coefficient does not

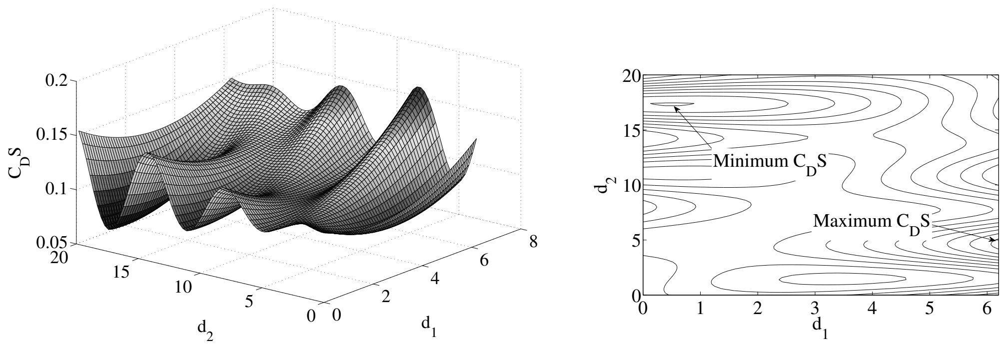

(a) 3D representation of the C_DS function

(b) Level curve representation of the C_DS function

Fig. 2 Deterministic values of C_DS shape coefficient as function of design variables d_1 and d_2

depend on the operational conditions, but only on the shape), $n_{gl} = Inf$ (with only 1 fidelity level); $n_{gcyc} = 3$; $d_{min,sl} = 0.1$ (all the inputs are normalized to $[-1, 1]$); $d_{min,ll} = 0.2$. Since the coefficient C_DS is considered only function of the shape, the generic row j of the matrix database used to train the ANN is $\mathbf{DB}_{train,j} = [d_1, d_2]$. The initial approximated model of C_DS was built with 30 samples, selected with a randomized Latin Hypercube. For such a small database, the learning procedure for the initialization of the approximating ANN was not able to properly converge to a good representation of the C_DS function. The evolution control added other 29 solutions (for a total of 59 model computations) and brought the approximated model to converge to the correct values of the C_DS function in the regions of interest, enabling the optimizer to converge to the expected optimal solutions. Fig. 3(a) shows the level curves of the approximated model at the last iteration of the EC together with the final population. Fig. 3(b) shows the final approximation to the Pareto front. The structure of the approximated C_DS function in Fig. 3(a) is almost identical to the true one in Fig. 2(b) and the maximum and minimum values are correctly identified. Individual *Best* σ_h^2 is not perfectly located at the position of the maximum of the function, but the achieved approximation is sufficient to make a correct decision on the design solution with best performance and with highest robustness. The relative error between the ANN approximated model and the true C_DS function at the locations of the individuals of the final population is shown in Fig. 4: if the initial ANN is considered, the relative error has an average value of more than 10%, on the other hand, when the final ANN is used, the error is almost always smaller than 3%, which is the required convergence level for the ANN learning process. The higher error displayed by individual 11 means that the value corresponds to a newly founded solution and that the ANN had not time to properly learn the related portion of the search space.

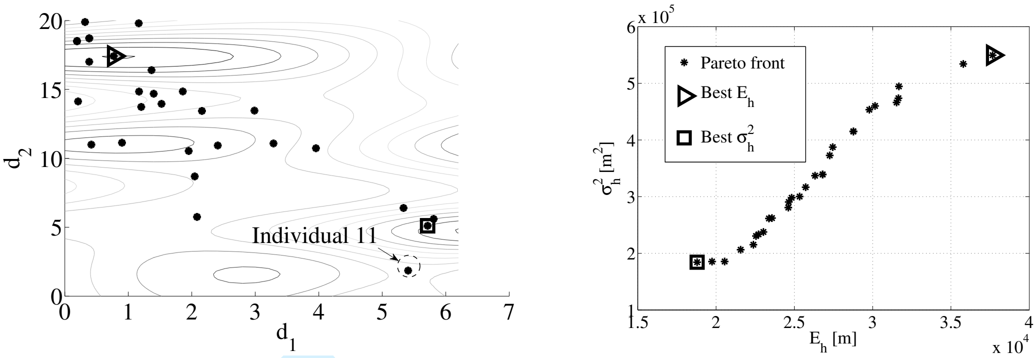

(a) Final population on level curve representation for C_DS approximated by ANN

(b) Pareto front approximation

Fig. 3 Results for the robust design optimization of rocket ascent case

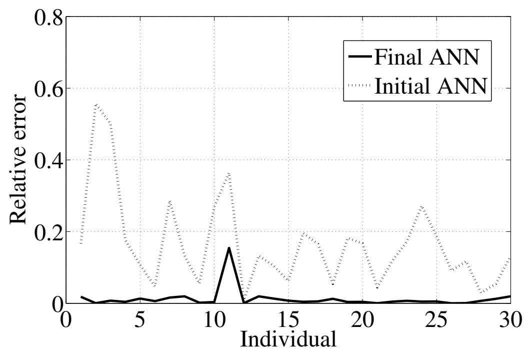

Fig. 4 Relative error between true C_DS function and ANN approximation for individual of final population

Although the deterministic control laws for the extreme best solutions (i.e. the one maximizing the expected values of the altitude E_h and the other minimizing the relative variance σ_h^2) appear similar as shown in Fig. 5(a), the differences in thrust profile and drag (Fig. 5(b)) allow them to follow different paths in the state space. Note that the obtained control laws well approximate the

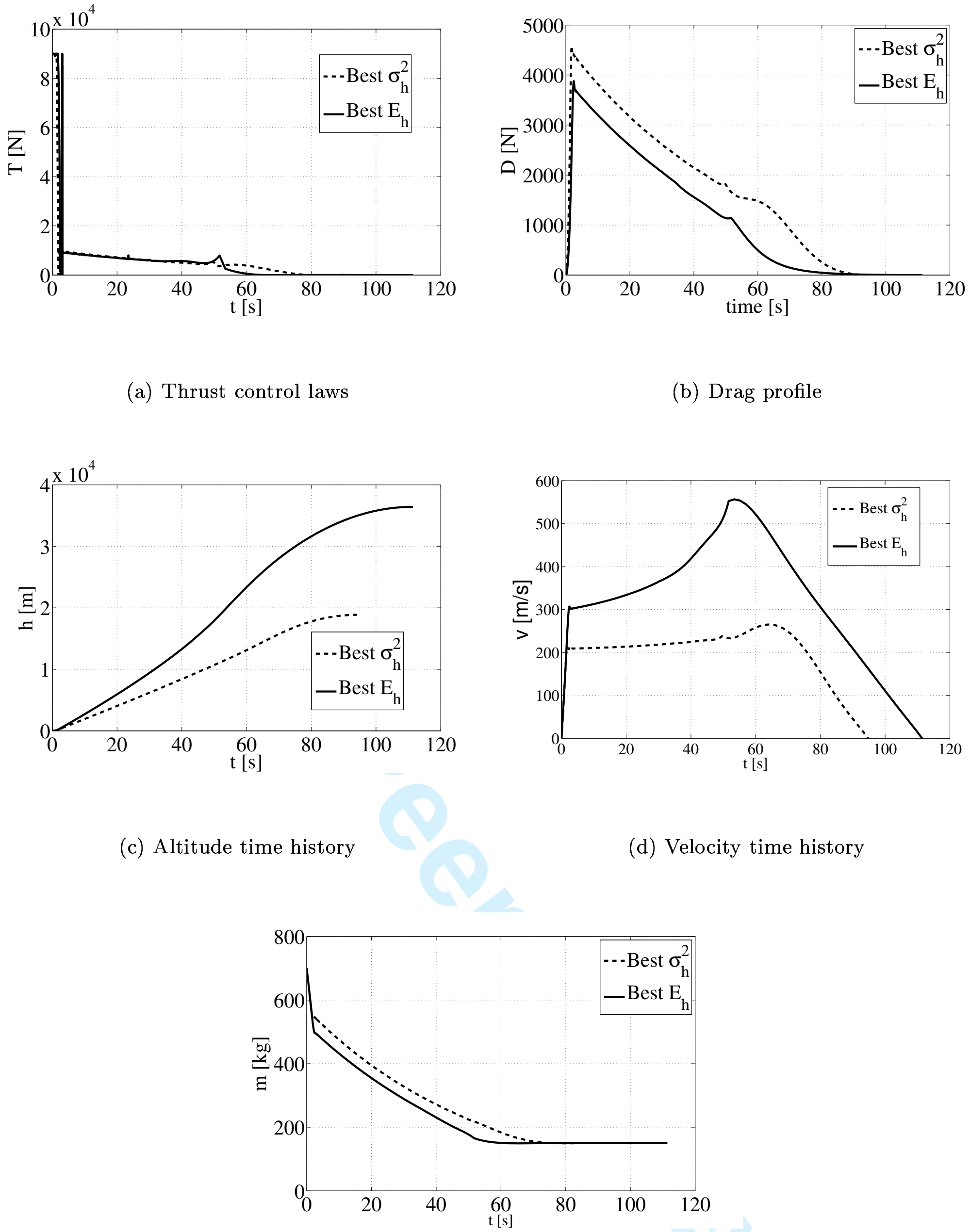

(a) Thrust control laws

(b) Drag profile

(c) Altitude time history

(d) Velocity time history

(e) Mass time history

Fig. 5 Results for the robust design optimization of rocket ascent case: best solutions

analytical solution that can be found in [39]. The solution with smaller $C_D S$ coefficient can climb higher and faster (see Figs. 5(c) and 5(d)). Due to a higher level of thrust during first few seconds of the climb, the solution with smaller $C_D S$ also has a faster consumption of mass, making it lighter for most of the trajectory (Fig. 5(e)). Since the uncertainty associated to the $C_D S$ increases with altitude and velocity (see Eq. (4)), then the best performing individual is also the least robust one. Vice versa, the least performing solution is less affected by uncertainties on the values of the shape parameters and thus is the most robust one.

IV. Unmanned Space Re-entry Vehicle Case Study

The goal of this case study is to design an Unmanned Space Vehicle (USV), for re-entry operations, that minimizes the maximum heat flux along the descent trajectory and maximizes the orthodromic distance measured on the Earth spherical surface. In the following, the system models for the design of the USV will be introduced before presenting the application of the proposed robust MDO process to this design case.

A. Geometry and Shape Model

The vehicle is a modified version of a waverider with rounded edges. The waverider baseline geometry is defined by three two-dimensional power-law equations[23]. The planform and the upper surfaces of the vehicle is parameterized by the length l, the width, w, a power law exponent n, the vehicle center line wedge angle, θ, and β, which is the oblique shockwave inclination angle[23]. An example can be found in Fig. 6, where the original waverider sharp-edge shape is modified to introduce a rounded edge with radius of curvature, $R_n > 0$. For the example in Fig. 6 the parameters defining the shape are: $l = 1.0m, w = 0.8m, n = 0.3, \theta = 10deg, \beta = 12deg, R_n = 0.02m$, and more details can be found in the cited reference.

B. Aerodynamic Models

Two different models are used to predict the aerodynamic characteristics of the vehicle. The former one is a simplified analytical model, which is here applied to the actual rounded-edge vehicle, although it was originally developed to predict the aerodynamics of the original sharp-edge shape of the waverider configuration[23]. It gives a very first approximation of the performance at the early stage of the design process. The latter one is a full high-fidelity CFD model based on a finite volume integration of Reynolds Averaged Navier-Stokes equations (RANS).

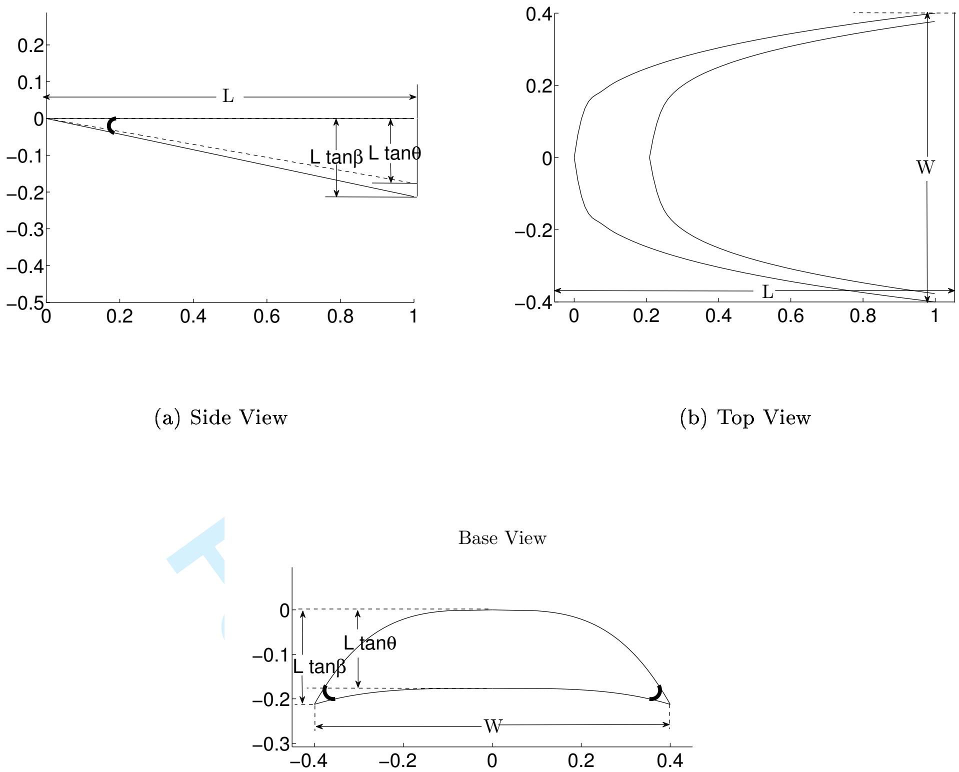

(a) Side View (b) Top View

(c) Base View

Fig. 6 Example of Vehicle Geometry: $l = 1.0m, w = 0.8m, n = 0.3, \theta = 10deg, \beta = 12deg, R_n = 0.02m$

1. Analytic Hypersonic Model

The analytic model gives the lift L and wave drag D_w as functions of the pressure on the upper, lower and base surfaces, P_u, P_l and P_b, respectively:

$$\begin{cases} L = S_b(P_b - P_l)sin\alpha + S_p(P_b - P_l)cos\alpha \\ D_w = S_b(P_l - P_b)cos\alpha + S_p(P_l - P_u)sin\alpha \end{cases} \tag{13}$$

where S_p and S_b are the planform area and the area of the base, computed as:

$$\begin{cases} S_p = \dfrac{wl}{n+1} \\ S_b = S_p tan(\theta) \end{cases} \tag{14}$$

The pressure on the surfaces can be calculated analytically with the oblique shock theory or Prandtl-Meyer expansion theory.[29] The viscous drag D_v is given in analytical form by using the

Table 2 Viscous drag constants for wedge-derived waverider

Constants	Laminar flow	Turbulent flow
G_1	$0.664\sqrt{\rho_e^2 v_e^3 \mu^* C^*/\rho^*}$	$0.037 v_e^{1.8}(\rho^*)^{0.8}(\mu^*)^{0.2}$
G_2	0.5	0.8
F_0	0.99845	0.99758
F_1	-0.57529	-0.80941
F_2	0.36737	0.54989
F_3	-0.11939	-0.18247

reference temperature method[30] as:

$$D_{v,surf} = G_1 w F(n) \left(\frac{l}{cos\theta_{surf}}\right)^{G_2} \tag{15}$$

with $F(n) = F_0 + F_1 n + F_2 n^2 + F_3 n^3$, and θ_{surf} is the inclination angle for the considered surface (upper or lower surface). The adopted constants, which depends on the flow conditions, are given in Table 2.

In Table 2, the Chapman-Rubensin parameter $C^* \approx (T_*/T_e)^{-\frac{1}{3}}$, ρ^*, and μ^* are determined by Eckert's empirical relation and Sutherland viscosity law, while ρ_e, T_e and v_e are the density, the temperature and the flow velocity at edge of boundary layer in post-shock conditions.

The total drag D is $= D_w + D_{v,u} + D_{v,l}$, where $D_{v,u}$ and $D_{v,l}$ are the viscous drag of the upper and lower surface, respectively.

As previously anticipated, this simplified model still considers the sharped shape of the wave rider, and does not take into account the modified one, with the introduction of the rounded edges.

2. CFD Model

On the other hand, a commercial code ($Numeca^{®}$), solving the Reynolds Averaged Navier-Stokes (RANS) equations, is used to obtain what are considered high fidelity solutions in the entire flight envelope and also to compute initial solutions when the analytical model could not be applied (for supersonic flight regimes).

The computational domain is discretized by a multi-block structured mesh made by 13 blocks with near 2.4 10^6 total nodes. For each configuration, the mesh is changed and adapted to the current geometry by internal scripting on the basis of design parameters. Since no out of plane flight conditions are considered, only half of the actual domain is discretized and mirror plane conditions are imposed into the longitudinal plane.

Two different settings are implemented and used during the process: a) Laminar for Reynolds number, Re, $< 0.95\ 10^5$; and b) Fully turbulent (no transition model is considered) for $Re > 1.05\ 10^5$.

For hypersonic conditions the radiative equilibrium temperature at the nose is imposed on the solid boundaries. Real gases database is enhanced on the basis of reported air data for high temperatures[31].

No solutions are computed for $0.95\ 10^5 \leq Re \leq 1.05\ 10^5$, in order to have an aerodynamic database as smooth as possible: since there is no transition model between laminar and turbulent flow, then computations into the transition region could be misleading. The data base will be approximated by a smooth ANN system, and then the ANN itself will provide smooth approximations for the transition region.

C. TPS and Thermal Model

The thermal protection system (TPS) is assumed to be made of Zirconium Diboride (ZrB_2) UHTC, which has following properties: density $= 6000 kg/m^3$, specific heat $= 628 JKg^{-1}K^{-1}$, conductivity $= 66 Wm^{-1}K^{-1}$, and emissivity $= 0.8$.

We bound the angle of attack to a maximum value of 20 deg, hence the highest heat flux is expected to be at the USV nose cap. Thus, the whole nose cone is made of UHTC with length L_{TPS}. The rest of the vehicle is covered with a thin shell with a constant thickness of 0.003 m.[32]

For the design process, the convective heat flux is computed in the simplest way, with the analytical formula[33]:

$$\dot{q}_{conv} = K_e \sqrt{\frac{\rho_\infty}{R_n}} V_\infty^3 \tag{16}$$

where $K_e = 1.742\ 10^{-4}$ (for the heat flux $\dot{q}_{conv}$ in W/m^2). As previously stated, the minimization of maximum heat flux means that less protecting material could be used, with consequent reduction of building costs.

D. Mass Model

The total mass of the vehicle is made of the structural mass m_{st}, the mass of the TPS m_{TPS}, and the mass of the payload (avionics and power system) m_{pl}.

$$m = m_{TPS} + m_{st} + m_{pl} \tag{17}$$

The mass of the payload is here assumed to be 40% of the structural mass, therefore $m_{pl} = 0.4\, m_{st}$. The mass of the TPS is made of the mass of the nose $m_{nose} = \rho_{TPS} V_n$ plus the mass of the thin skin covering the rest of the vehicle m_{skin}, where V_n, is the volume of the nose and ρ_{TPS} the density of the TPS material. The mass of the TPS skin covering the vehicle, except the nose, is:

$$m_{skin} = \rho_{TPS}\, S_{TPS}\, d_{TPS} \tag{18}$$

where d_{TPS} is the thickness of the TPS , and S_{TPS} is surface area except that of the nose, which can be approximated by $S_{TPS} = 2S_{pE} + S_{bE} - S_n$ (S_{pE} and S_{bE} are the total planform surface and the area of the rear part of the rounded edge waverider, respectively, and S_n is the surface of the TPS nose).

The structure of the vehicle is supposed to be made of titanium, with a density of 4400 kg/m^3. The structural mass m_{st}, can be obtained from:

$$m_{st} = \rho_{\text{body}}(2S_{pE} + S_{bE})d_{body} \tag{19}$$

where, in this case, d_{body}= 0.005 m is the thickness of the structure of the vehicle, seen as a shell.

E. Dynamic Equations

The vehicle is considered to be a point mass, whose motion is governed by the following set of dynamic equations[34]:

$$
\begin{aligned}
\dot{r} &= v sin\theta_p \\
\dot{\lambda} &= \frac{v cos\theta_p cos\xi}{r cos\phi} \\
\dot{\phi} &= \frac{v cos\theta_p sin\xi}{r} \\
\dot{v} &= -\frac{D(\alpha)}{m} - g sin\theta_p \\
\dot{\theta}_p &= \frac{L(\alpha)}{mv} cos\gamma_v - (\frac{g}{v} - \frac{v}{r}) cos\theta_p \\
\dot{\xi} &= \frac{L(\alpha)}{mv cos\theta} sin\gamma_v - \frac{v}{r}\cos\theta_p \cos\xi \tan\phi
\end{aligned}
\tag{20}
$$

where r is the norm of the position vector with respect to the center of the planet, λ is the longitude, ϕ the latitude, v the magnitude of the velocity, θ_p is the flight path angle, ξ is the heading angle (azimuth of the velocity). No out of plane maneuvers are considered, thus the bank angle γ_v is kept equal to zero during the whole trajectory.

F. USV Optimization Set-Up

As for the previous test case, the outer multi-objective evolutionary procedure manages the parameters defining the shape of the vehicle and considers as objectives and constraints the mean and variance of the values of performance indexes of inner optimal control processes. On the other hand, now the optimal control problem is solved twice, first to minimize the maximum heat flux, $\max_t \dot{q}$, and then to maximize the orthodromic distance, $Dist$. Mean and variance of these two performance indexes are then computed following the procedure described in Sec. II B. The optimal control sub-problem, considering deterministic models, gives deterministic values of the performance indexes, $\max_t \dot{q}$ and $Dist$, as a function of the optimal α profile. However, a number of elements can be considered uncertain, such as the aerodynamic forces and the mass. Therefore, one can associate to the nominal value of lift L_{det} and drag D_{det}, the uncertain quantities:

$$
\begin{aligned}
L_{unc} &= L_{det} + Err(\alpha, v, h) C_E(\alpha, v, h) L_{det} \\
D_{unc} &= D_{det} + Err(\alpha, v, h) C_E(\alpha, v, h) D_{det}
\end{aligned}
\tag{21}
$$

where the error function Err depends on the angle of attack, the speed and the altitude h, and the sampling function C_E maps a triplet of values of angles of attack, speed and altitude into the interval $[-1, 1]$. As it was done in Sec. III, the uncertainties in the aerodynamic model are assumed to be increasing with angle of attack, speed, and altitude, thus Err is modeled as a linear 3D surface, with values that vary from 0.2, when angle of attack, speed and altitude are $= 0$, to 0.8, when the incidence is $= 20\ deg$, the speed is $= 8000\ m/s$ and the altitude is $10^5\ m$:

$$Err = 0.01\,\alpha + 2.5\,10^{-5}\,v + 2\,10^{-6}\,h + 0.2 \tag{22}$$

The C_E functions is again built as a combination of splines with equidistant nodes. In this case their shape is given by:

$$C_E = Sp_\alpha(\alpha,\, \mathbf{s}_\alpha)\; Sp_h(h,\, \mathbf{s_h})\; Sp_v(v,\, \mathbf{s_v}) \tag{23}$$

where $Sp_\alpha(\alpha,\, \mathbf{s}_\alpha)$, $Sp_h(h,\, \mathbf{s_h})$ and $Sp_v(v,\, \mathbf{s_v})$ are the splines for angle of attack, altitude and velocity, respectively. The total mass is considered uncertain as well, and it is assumed that m can uniformly vary in the range ± 0.1 of the reference value. Then, given a nominal trajectory with an optimal control profile α^*, N_s varied trajectories are propagated, and the mean and the variance of $\max_t \dot{q}$ and $Dist$ are computed from the N_s values of $\max_t \dot{q}$ and $Dist$, one for each varied trajectory.

G. Shape Optimization

If one calls $E_{q,1}$ and $\sigma^2_{q,1}$ the mean value and variance of maximum heat flux, and $E_{D,1}$ and $\sigma^2_{D,1}$ the mean value and variance of the orthodromic distance after the first control optimization (considering the maximum heat flux as objective to minimize), and $E_{q,2}$, $E_{D,2}$, $\sigma^2_{q,2}$, $\sigma^2_{D,2}$ the corresponding values after the second control optimization (considering the orthodromic distance as objective to maximize), then the external process is set as:

$$\min_{\mathbf{d} \in D} [E_{q,1},\; -E_{D,2},\; \sigma^2_{q,1} + \sigma^2_{q,2}] \tag{24}$$

subject to the following constraints:

$$\begin{aligned} &E_{q,1} \le \bar{E}_q \\ &(\sigma^2_{q,1} + \sigma^2_{q,2}) \le \bar{\sigma}^2_q \end{aligned} \tag{25}$$

while the design vector $\mathbf{d}$ is defined as $\mathbf{d} = [l, w, n, \theta, R_n, \Delta\dot{q}]$ (the meaning of $\Delta\dot{q}$ is explained in the next section). Note that, as previously mentioned, the external optimizer needs to work on objectives representing the best performance of the shape, for both different cases.

The design space for problem(24,25) is defined by the following bounds on the design parameters: the nominal length $l \in [2.9, 4.2][m]$, the nominal width $w \in [1.0, 2.0][m]$, the exponent $n \in [0.2, 0.7]$, the angle $\theta \in [7, 11][deg]$, the radius of the nose $R_n \in [0.01, 0.04][m]$, the constraint on the maximum heat flux for the second control law optimization $\Delta\dot{q} \in [20, 70][W/cm^2]$. The angle β, as defined in Sec. IV A, is kept fixed to $12deg$. Moreover, here L_{TPS} is not considered as a design parameter, and its value is set as 10% of the effective length of the vehicle. The constraints on the external process are: $\bar{E}_q = 180$ and $\bar{\sigma_q^2} = 1000$.

H. Trajectory Optimization

For the trajectory optimization problem, the control variable is the angle of attack α. Two control laws are computed as the result of the two optimal control subproblems:

$$\min_{\alpha}\left(\max_{t}\dot{q}\right) \quad and \quad \max_{\alpha} Dist \tag{26}$$

both subject to dynamic equations (20) and terminal conditions:

$$\begin{aligned}
&r(t=0) = r_0\\
&\lambda(t=0) = \lambda_0\\
&\phi(t=0) = \phi_0\\
&v(t=0) = v_0\\
&\theta_p(t=0) = \theta_0\\
&\xi(t=0) = \xi_0
\end{aligned} \tag{27}$$

$$\begin{aligned}
&r(t=t_f) \le r_f\\
&r(t=t_f) \ge r_{min}\\
&v(t=t_f) \le v_f\\
&v(t=t_f) \ge v_{min}
\end{aligned} \tag{28}$$

As for rocket ascent case, these problems are transcribed with a Gauss pseudo-spectral method, and after transcription, the optimal control problems defined by Eqs. (20) and (26, 27, 28) become the following general nonlinear programming problem:

$$\min_{\alpha_s}\left(\max_t \dot{q}\right) \;\; and \;\; \max_{\alpha_s} Dist \tag{29}$$

subject to the nonlinear algebraic constraints:

$$C(r_s, \lambda_s, v_s, \xi_s, \theta_s, \alpha_s, t_s) = 0 \tag{30}$$

and the terminal constraints (27, 28), where r_s, λ_s, ϕ_s, v_s, ξ_s, θ_s, α_s, t_s are the discrete values of the time, states and control values at the nodes of the transcription scheme. In order to obtain feasible solutions that can be integrated, an inequality constraint on the variation of the control law is also imposed: for each node the slope of the control law $\leq \Delta\alpha$.

Note that the second optimization problem takes into account an additional constraint on the maximum heat flux, which should be $\leq (\dot{q}_{max,1} + \Delta\dot{q})$, where $\dot{q}_{max,1}$ is the deterministic value of the maximum heat flux resulting from the previous control law optimization, and $\Delta\dot{q}$ is a variable of the problem, managed by the external evolutionary process. The re-entry time is free and no other terminal conditions are imposed as there is no specific requirement on the landing point.

The trajectories are discretized with 6 elements, and 12 nodes are considered for the first 3 elements (from starting point to half of the trajectory path), where maximum values of the heat flux and major trajectory oscillations are expected, while 5 nodes are considered for the other 3 elements. The bounds on the variables of the trajectory optimization are: total time $T_{tot} \in [500, 6500]$ $[s]$, angle of attack $\alpha \in [0, 20]$ $[deg]$, radius $r \in [6.380\ 10^6, 6.480\ 10^6][m]$, longitude $\lambda \in [-180, 21]$ $[deg]$, latitude $\phi \in [-90, 68]$ $[deg]$, speed $v \in [100,\ 10^4]$ $[m/s]$, flight path angle $\theta_p \in [-80, 10]$ $[deg]$, heading angle $\xi \in [-225, -90]$ $[deg]$.

The initial conditions (27) are $x_0 = [R_E +\ 10^5,\ 21,\ 68,\ 7700,\ -0.3,\ -145]^T$, where R_E is the mean radius of the Earth, while the constraints on the final conditions are $r_f = R_E + 50000$ m, $r_{min} = R_E + 15000$ m, $v_f = 1100$ m/s, $v_{min} = 900$ m/s, while the slope of the control law is $\Delta\alpha = 1/10$ deg/s. The initial guess of the control law for every individual had 18 deg incidence at time $t = 0$, linearly decreasing, with decrements $d\alpha = 1/1000$ deg/s, till the last point of the trajectory obtained by direct integration satisfies the constraints on the required final velocity and altitude. Note that, when the optimal control process does not converge, the initial guess of the control law is considered.

I. USV Results

The MOO process was run for 60 generations with a population of 60 individuals. It should be noted that number of generations and individuals was chosen as a compromise between the expected amount of function evaluations to converge and the available computational time, and due to the stochastic nature of the search there could be no proof on the convergence to the global Pareto set. The initial approximated models were built with 1000 samples, selected with a randomized Latin Hypercube, coming from 920 analytic model computations and additional 80 supersonic CFD computations to have an extended range of validity, without the need to excessively extrapolate. The computation of the first database required nearly 1200 hours of computational time, distributed on a cluster of 20 linux64 processors (near 3 days of effective time). The computations of the CFD solver were stopped when convergence was obtained on the aerodynamic forces.

The characteristic parameters of the evolution control process were set as follows: $n_t = n_o = 20$, $n_{gl} = 10$, with only 1 switch; $n_{gcyc} = 5$; $d_{min,sl} = 0.3$ (all the inputs are normalized to $[-1, 1]$); $d_{min,ll} = 0.8$. Since in this case the aerodynamic characteristics of the vehicle are functions of both shape and operational conditions, the generic row j of the database used to train the ANN is $\mathbf{DB}_{train,j} = [l,\, w,\, n,\, \theta,\, R_n,\, v,\, h,\, \alpha]$.

At level 0, which is considered up to generation 10, CFD computations were used to verify only supersonic points, while at level 1, which is considered from generation 11, CFD computations were used to verify the trajectory points for the whole trajectory.

During the computation, until generation 50, solutions obtained with the CFD model increased up to 250, all allocated in the promising region of the search space. On the other hand, analytical solutions used to build the ANN approximated models decreased to nearly 500. From generation 50 to 60 no more new verified values are added to the ANN database.

The approximation of the Pareto front at the end of the optimization process is shown in Fig. 7.

As expected, the front is sparse and irregular, due to the nature of the objective functions, which are extremely noisy because they are the outcome of the Monte-Carlo simulation ($N_s = 300$, then each individual required 600 re-propagations). Moreover, the speed and accuracy of convergence of the trajectory optimization loop is quite sensitive to shape parameters and initial conditions. A different population size could improve the quality of the front although a trade-off between exhaustiveness of the search and computational resources is required.

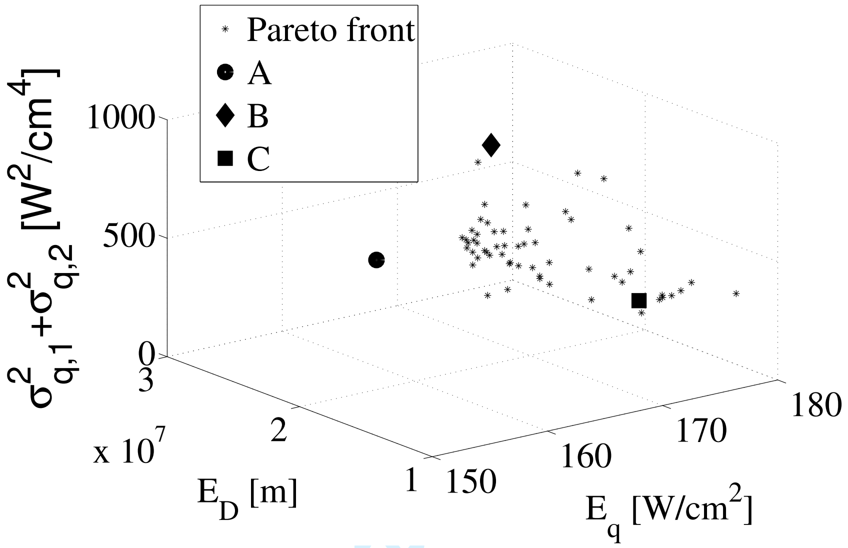

Fig. 7 Approximation of the Pareto front at the end of the optimization process

In Fig. 8 individuals A, B, and C minimize the mean value of the maximum heat flux, maximize the mean value of the distance, and minimize the sum of the variances, respectively. The design parameters for solutions A, B and C are:

1. Solution A: $l = 2.93998; w = 1.19734; n = 0.6977; \theta = 9.9983; R_n = 0.03532; \Delta\dot{q} = 41.9184$
2. Solution B: $l = 2.98669; w = 1.28207; n = 0.6871; \theta = 10.4961; R_n = 0.03719; \Delta\dot{q} = 62.6298$
3. Solution C: $l = 3.12287; w = 1.49396; n = 0.6999; \theta = 9.7599; R_n = 0.03913; \Delta\dot{q} = 33.8409$

The optimization is mainly driven by the heat flux and its variance. In order to limit the heat flux at the nose, the algorithm searches for solutions with a relatively large radius of the nose, and small dimensions. Since the total mass is strictly related to the size, small vehicles are also light weighted and can glide at higher altitude avoiding the very critical part of the flight envelope. A

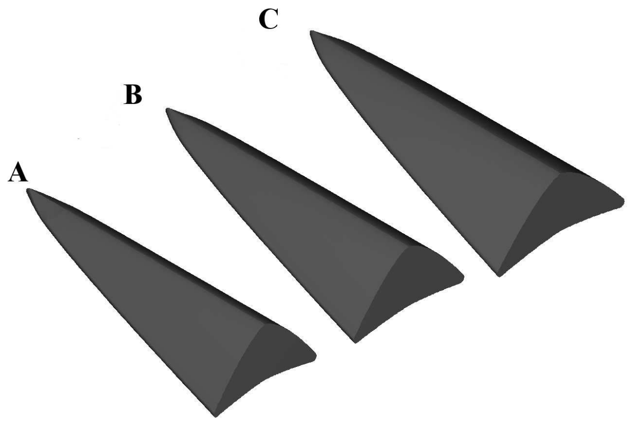

Fig. 8 Optimal solutions: individual A minimizes the mean value of the maximum heat flux, individual B maximizes the mean value of the achievable distance, while individual C minimizes the sum of the variances.

reduction in size, however, could reduce the lift and drag which are required to remain high to glide and dissipate energy over an extended period of time. The result is that short vehicles, that do not sacrifice wingspan to reduce weight, provide acceptable performance and good robustness against uncertainties on the heat flux. All final solutions appear belonging to the same shape niche, but have quite different masses, which are determined by geometrical characteristics. Likely the convergence to the shape niche is due to the stronger influence of the vehicle mass on the optimization of the trajectory.

Fig. 9 shows the nominal, deterministic trajectories of the three selected individuals, when the control law is optimized taking into account the maximum heat flux as performance index. The shapes of the individuals are very similar (meaning similar aerodynamic performance), but the smaller size, meaning a smaller mass as well, allows individual A to follow a higher re-entry path in the critical part of the trajectory, limiting the heat loads (Fig. 10) (the masses of individuals A, B, and C are 191, 212, 248 kg, respectively).

Fig. 11, where the angle of attack is plotted against time, shows small differences in the profile of the angle of attack (less than three degrees in the initial part of the descent). These differences together with the differences in the system design produce a relevant effect on the trajectory and

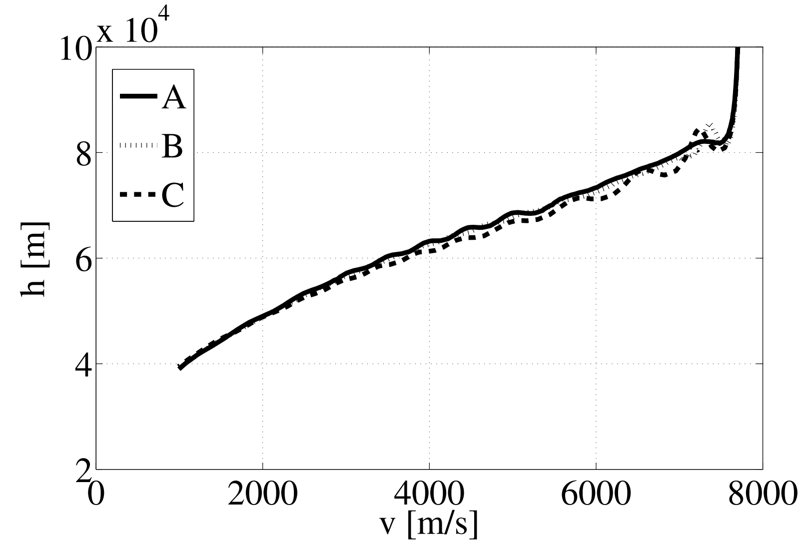

Fig. 9 Trajectories of the selected optimal solutions.

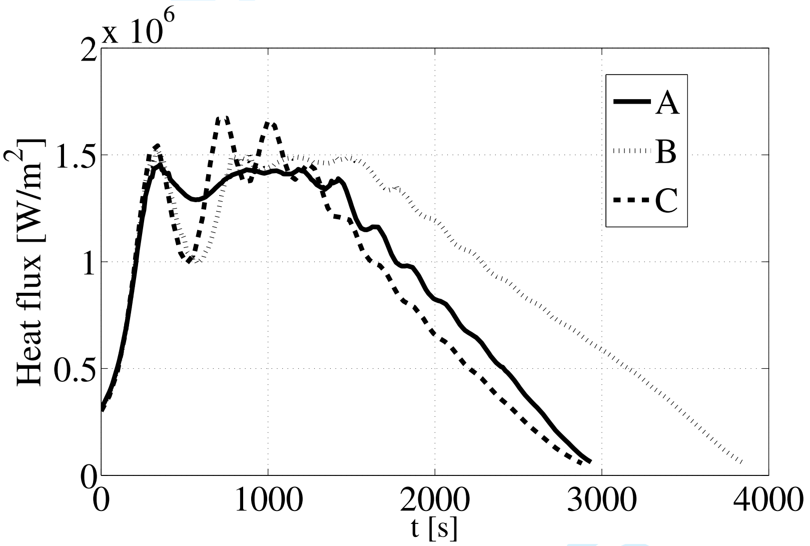

Fig. 10 Convective heat flux of the selected optimal solutions.

on the heat flux.

In order to appreciate the difference between the outcome of the robust optimization process and non-robust solution, a second bi-objective optimization, which only considers the deterministic values of the maximum heat flux and the orthodromic distance as objectives, has been carried out. The deterministic optimization has been carried out with the same bounds, and same MOPED settings of the robust one. The approximated Pareto front is shown in Fig. 12, and compared to

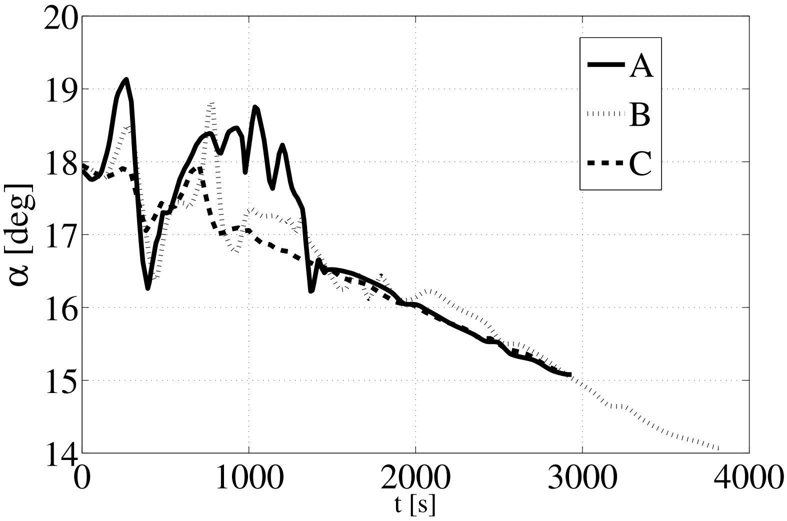

Fig. 11 Angle of attack control law.

a 2D projection of the robust one. As expected the process is able to find solutions with smaller (better) values of the maximum heat flux (left part of the figure), which, in the robust case, are not Pareto optimal because of the third objective function. It has to be noted, however, that this particular run is not capturing the part of the front, which should be expected above individuals A and B. This partial coverage is due to the stochastic nature of the evolutionary process and the noise in the model, even if in the case of deterministic process, the noise is only associated to the convergence of the control law optimization process, since MC simulation is not required. Again, due to the stochastic nature of the optimization process, a rigorous comparison between deterministic and robust solution would require multiple runs to capture the statistical variability of the result. Such an analysis is extremely computationally expensive and out of the scope of this paper.

V. Conclusions

This paper described a novel evolutionary approach to integrate system design and optimal control into a single optimization process. The procedure implements a combination of a global, population-based solver with a direct transcription method for optimal control problems.

The proposed approach is applied to two different test cases: the robust design of a single-stage vertically ascending rocket and the robust design of a small scale USV for re-entry operations. In

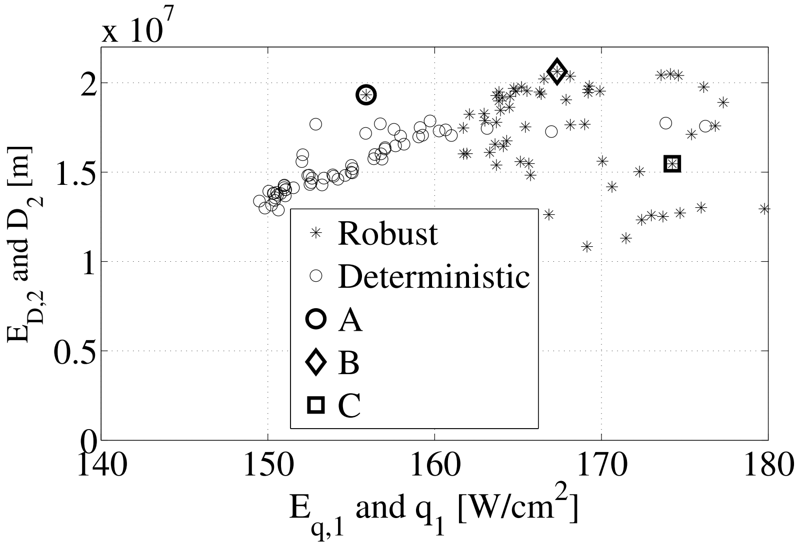

Fig. 12 Comparison between robust and deterministic optimization processes.

both cases, the optimal control solver is interfaced with an ANN, approximating the aerodynamic forces as a function of the geometric parameters and operational conditions. The paper showed that the training and updating of the ANN, by the proposed form of evolution control, converges to a correct representation of the true models in the regions of interest. In the rocket ascent case, the surrogate model could be verified to correctly represent the true model with a final relative error below 3%. On the same case, the MDO process was able to correctly identify the best performing and most robust design solutions under uncertainty. The use of a surrogate allowed for an efficient integration uncertainties on the dynamic models (in particular the aerodynamic forces). For the USV test case, the evolution control procedure was extended to manage and integrates models at different levels of fidelity. Even if the USV model presented in this paper is not fully comprehensive of all the aspects defining the system and phenomena occurring during the re-entry phase, nonetheless it has the main characteristics of a real, complex case, such as: the system and optimal control components are integrated in a multilevel design optimization process, both system and optimal control design processes are computationally expensive and very noisy.

In the future, the approach will be tested on more realistic re-entry problems and generalized to solve analogous problems in other engineering fields, e.g. the design of chemical plants and the design of high performance cars for predefined circuits, also with higher number of shape design variables, at the limits of the meta-modeling capabilities.

The current work is mainly focused on the improvement of the aero-thermodynamic model to insert also unsteady computations into the process. These additional computations are likely to be needed only for few points of the flight envelope to better assess the errors, and consequent uncertainties, when lower fidelity models are adopted. The uncertainty modeling is currently one of the most critical aspects of the system and needs to be improved including knowledge coming from the expected error of the approximated model and convergence level of the CFD results.

Other important aspects to consider for future improvements are the techniques for model approximation and the convergence of the internal optimal control solver, which are crucial for the correct convergence of the evolutionary process towards optimal shapes.

References

[1] Tsuchiya, T., "An Integrated Optimization for Conceptual Design of Spaceplane," *22nd Congress of International Council of the Aeronautical Sciences*, Harrogate, UK, 28 August - 1st September 2000.

[2] Tsuchiya, T. and Mori, T., "Multidisciplinary Design Optimization to Future Space Transportation Vehicles," *AIAA/AAAF 11th International Space Planes and Hypersonic Systems and Technologies Conference*, Orleans, France, 29 September - 4 October 2002.

[3] J.Roshanian and Z.Keshavarz, "Effect of Variable Selection on Multidisciplinary Design Optimization: a Flight Vehicle Example," *Chinese Journal of Aeronautics*, Vol. 20, No. 1, 2006, pp. 86–96. doi10.1016/S1000-9361(07)60012-0.

[4] Alexandrov, N., Lewis, R., Gumbert, C., Green, L., and Newman, P., "Approximation and model management in aerodynamic optimization with variable-fidelity models," *Journal of Aircraft*, Vol. 38, No. 6, 2001, pp. 1093–1101. doi10.2514/2.2877.

[5] Shyy, W., Papila, N., Vaidyanathan, R., and Tucker, K., "Global design optimization for aerodynamics and rocket propulsion components," *Progress in Aerospace Sciences*, Vol. 37, 2001, pp. 59–118.

[6] Giannakoglou, K., "Design of optimal aerodynamic shapes using stochastic optimization methods and computational intelligence," *Progress in Aerospace Sciences*, Vol. 38, No. 1, 2002, pp. 43–76. doi: 10.1016/S0376-0421(01)00019-7.

[7] Ong, Y., Nair, P., and Keane, A., "Evolutionary Optimization of Computationally Expensive Problems via Surrogate Modelling," *AIAA Journal*, Vol. 41, No. 4, 2003, pp. 687–696.

doi: 10.2514/2.1999.

[8] Keane, A. and Nair, P., *Computational Approaches for Aerospace Design: The Pursuit of Excellence*, John-Wiley and Sons, 2005.

[9] Forrester, A., Sobester, A., and Keane, A., *Engineering Design via Surrogate Modelling: A Practical Guide*, John-Wiley and Sons, 2008.

[10] Lozano, J. A., Larranaga, P., and Inza, I., *Towards a New Evolutionary Computation: Advances on Estimation of Distribution Algorithms (Studies in Fuzziness and Soft Computing)*, Springer, February 2006.

[11] Costa, M. and Minisci, E., "MOPED: a Multi-Objective Parzen-based Estimation of Distribution algorithm," *Evolutionary Multi-Criterion Optimization. Second International Conference, EMO 2003*, edited by C. Fonseca, P. Fleming, E. Zitzler, K. Deb, and L. Thiele, Vol. 2632 of *LNCS*, Springer, Faro, Portugal, 08-11 April 2003, pp. 282–294.

[12] Avanzini, G., Biamonti, D., and Minisci, E., "Minimum-Fuel/Minimum-Time Maneuvers of Formation Flying Satellites," *Astrodynamics Specialist Conference*, AAS 03-654, Big Sky, Montana, 03-07 August 2003.

[13] Betts, J. T., *Practical Methods for Optimal Control and Estimation Using Nonlinear Programming, Second Edition*, SIAM, 2010.

[14] Jin, Y., Olhofer, M., and Sendhoff, B., "A Framework for Evolutionary Optimization with Approximate Fitness Functions," *IEEE Transactions on Evolutionary Computation*, Vol. 6, No. 5, 2002, pp. 481–494. doi: 10.1109/TEVC.2002.800884.

[15] Russo, G. and P.P. De Matteis, "PRORA-USV: Two Flight Mission Exploring Transonic Conditions," *Proccedings of the 15th AIAA International Space Planes and Hypersonic Systems and Technologies Conference*, AIAA 2008-2660, Dayton, Ohio, USA, 2008.

[16] Savino, R. and Serpico, D. P. M., "Numerical and Experimental Investigation of PRORA USV Subsonic and Transonic Aerodynamics," *Journal of Spacecraft and Rockets*, Vol. 43, No. 3, 2006, pp. 575–584. doi: 10.2514/1.12352.

[17] Russo, G., "USV Program Status 2009," *Proceedings of the 16th AIAA/DLR/DGLR International Space Planes and Hypersonic Systems and Technologies Conference*, AIAA-2009-7269, Wahington, DC, 2009.

[18] Minisci, E., Liqiang, H., and Vasile, M., "Multidisciplinary Design of a micro-USV for Re-entry Operations," *AIAA Guidance, Navigation, and Control Conference*, AIAA 2010-7968, Toronto, Ontario Canada, 02-05 August 2010.

[19] Viviani, A. and Pezzella, G., "Heat Transfer Analysis for a Winged Reentry Flight Test Bed," *Interna-*

tional Journal of Engineering, Vol. 3, No. 3, 2009, pp. 330–345.

[20] Squire, T. and Marschall, J., "Material property requirements for analysis and design of UHTC components in hypersonic applications," *Journal of European Ceramic Society*, Vol. 30, No. 1, 2010, pp. 2239–2251.
doi: 10.1016/j.jeurceramsoc.2010.01.026.

[21] Strohmeyer, D., Eggers, T., and Haupt, M., "Waverider Aerodynamics and Preliminary Design for Two-Stage-to-Orbit Missions, Part 1," *Journal of Spacecraft and Rockets*, Vol. 35, No. 4, 1998, pp. 450–458.
doi: 10.2514/2.3375.

[22] Heinze, W. and Bardenhagen, A., "Waverider Aerodynamics and Preliminary Design for Two-Stage-to-Orbit Missions, Part 2," *Journal of Spacecraft and Rockets*, Vol. 35, No. 4, 1998, pp. 459–466.
doi: 10.2514/2.3376.

[23] Starkey, R. P. and Lewis, M. J., "Analytical Off-Design Lift-to-Drag-Ratio Analysis for Hypersonic Waveriders," *Journal of Spacecraft and Rockets*, Vol. 37, No. 5, 2000, pp. 684–691.
doi: 10.2514/2.3618.

[24] Robinson, T., Eldred, M., Willcox, K., and Haimes, R., "Surrogate-Based Optimization Using Multifidelity Models with Variable Parameterization and Corrected Space Mapping," *AIAA Journal*, Vol. 46, No. 11, 2008, pp. 2814–2822.
doi: 10.2514/1.36043.

[25] Singh, G. and Grandhi, R., "Mixed-Variable Optimization Strategy Employing Multifidelity Simulation and Surrogate Models," *AIAA Journal*, Vol. 48, No. 1, 2010, pp. 215–223.
doi: 10.2514/1.43469.

[26] Doherty, J. J., Dean, S. R. H., Ellsmore, P., and Eldridge, A., "A Multi-Fidelity Approach for Supporting Early Aircraft Design Decisions," *Collaborative Product and Service Life Cycle Management for a Sustainable World*, edited by R. Curran, S. Y. Chou, and A. Trappey, Springer London, London, 2008, pp. 267–279.

[27] Choi, S., Alonso, J., Kroo, I., and Wintzer, M., "Multifidelity Design Optimization of Low-Boom Supersonic Jets," *Journal of Aircraft*, Vol. 45, No. 1, 2008, pp. 106–118.
doi: 10.2514/1.28948.

[28] Choi, S., Alonso, J., and Kroo, I., "Two-Level Multifidelity Design Optimization Studies for Supersonic Jets," *Journal of Aircraft*, Vol. 46, No. 3, 2009, pp. 776–790.
doi: 10.2514/1.34362.

[29] Chapman, C., *High speed flow*, Cambridge University Press, 2000.

[30] White, F., *Viscous Fluid Flow*, McGraw-Hill, New York, 1974.

[31] Aupoix, B. and Cousteix, J., "Real Gas Effects in Two- and Three-Dimensional Hypersonic, Laminar Boundary Layers," *Computational Methods in Hypersonic Aerodynamics*, edited by T. Murthy, Kluwer Academic Publishers, 1991, pp. 293–340.

[32] Savino, R., De Stefano Fumo, M., Paterna, D., and Serpico, M., "Aerothermodynamic study of UHTC-based thermal protection systems," *Aerospace Science and Technology*, Vol. 9, 2005, pp. 151–160. doi: 10.1016/j.ast.2004.12.003.

[33] Anderson, J., *Hypersonic and High-Temperature Gas Dynamics (Second Edition)*, AIAA, 2006.

[34] Hankey, W. L., *Re-entry Aerodynamics (AIAA Education Series)*, AIAA, 1988.

[35] Deb, K., Pratap, A., Agarwal, S., and Meyarivan, T., "A Fast and Elitist Multiobjective Genetic Algorithm: NSGA-II," *IEEE Transaction on Evolutionary Computation*, Vol. 6, No. 2, april 2002, pp. 182–197.

[36] Fukunaga, K., *Introduction to statistical pattern recognition*, Academic Press, 1972.

[37] Fornberg, B., *A Practical Guide to Pseudospectral Methods*, Cambridge University Press, 1998.

[38] MacKay, D., "Bayesian interpolation," *Neural Computation*, Vol. 4, No. 3, 1992, pp. 415–447.

[39] Bryson, A.E., Ho, Y.C., *Applied optimal control: optimization, estimation, and control*, Taylor & Francis, 1975.